Solar Energy 262 (2023) 111819

Contents lists available at ScienceDirect

Solar Energy

journal homepage: www.elsevier.com/locate/solener

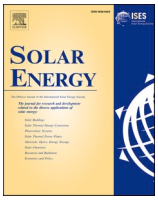

# A comprehensive methodological workflow to maximize solar energy in low-voltage grids: A case study of vertical bifacial panels in Nordic conditions

S. Jouttijärvi [a,b,*], J. Thorning [b,c], M. Manni [b], H. Huerta [d], S. Ranta [d], M. Di Sabatino [c], G. Lobaccaro [b], K. Miettunen [a]

[a] Department of Mechanical and Materials Engineering, Faculty of Technology, University of Turku, Turku, Finland
[b] Department of Civil and Environmental Engineering, Faculty of Engineering, Norwegian University of Science and Technology, Trondheim, Norway
[c] Department of Materials Science and Engineering, Faculty of Natural Sciences, Norwegian University of Science and Technology, Trondheim, Norway
[d] Unit of Chemical Industry, Turku University of Applied Sciences, Turku, Finland

ARTICLE INFO

*Keywords:*
Low-voltage grid
Vertical bifacial PV
High-latitude conditions
PV hosting capacity

ABSTRACT

The large-scale deployment of solar photovoltaic (PV) panels in residential and commercial buildings affects the local distribution grid. Voltage rises during times when PV production exceeds consumption can limit the hosting capacity of the distribution grid. This study presents a comprehensive methodological workflow that moves from the solar analysis of an ideal district to the identification of the PV hosting capacity of a distribution grid. The workflow aims to be highly flexible: the input parameters (i.e., PV technology, PV orientation, global horizontal solar irradiation, and grid properties) can be varied to simulate different cases and compare the corresponding hosting capacities. This workflow enables the analysis of the influences of PV systems' properties and orientation, electricity consumption, and grid characteristics on a grid's hosting capacity. A case study was conducted in which the IEEE European Low Voltage Test Grid was used, and conventionally mounted monofacial photovoltaic (MPV) panels were progressively replaced with east–west oriented, vertically mounted bifacial photovoltaic (VBPV) panels that can provide a better match with the electricity load and a higher daily total to daily peak electricity production ratio. The benefits of VBPV are highlighted at high-latitude locations, such as Nordic countries. Therefore, Turku, Finland, which is at a representative Nordic latitude considering the locations of the most important population centers, was chosen as the location for the case study. The results showed that applying VBPV increased a grid's PV hosting capacity significantly, up to 46% with the optimal system (30% MPV and 70% VBPV).

## 1. Introduction

The rapid increase in distributed photovoltaic (PV) installations in power systems has created challenges for power grid operators [11]. Voltage rise in distribution grids occurs when PV production exceeds electricity demand. Voltages that are too high can damage the grid and the electrical devices connected to it. Thus, the voltage must be restricted below a threshold either by identifying the distribution grid's maximum allowed PV capacity or by setting a limit to the maximum allowed PV production and curtailing excess production. The former approach causes severe restrictions to PV capacity, whereas the latter approach leads to loss of production.

To predict and mitigate voltage rises and other negative PV-induced effects (e.g., voltage unbalance, voltage flicker, harmonic currents, and rapid changes in demand for backup power), accurate modeling of both the expected PV power output and the effect of PVs on the local power grid are required. Ultimately, predicting and mitigating such effects enables higher PV production and reduces unwanted variations and instabilities that can shorten the lifetime of grid components. The solar irradiance impinging on the PV system at a specific location and panel orientation must be known to model the PV power output. Because measured values of global tilted irradiance (GTI) are rarely available, GTI is usually modeled based on global horizontal irradiance (GHI). GHI is divided into direct normal irradiance (DNI) and diffused horizontal irradiance (DHI) via decomposition modeling [34] and then converted

* Corresponding author at: Department of Mechanical and Materials Engineering, Faculty of Technology, University of Turku, Turku, Finland.
*E-mail address:* sami.jouttijarvi@utu.fi (S. Jouttijärvi).

https://doi.org/10.1016/j.solener.2023.111819
Received 28 June 2022; Received in revised form 21 February 2023; Accepted 23 June 2023
Available online 30 June 2023

**Nomenclature**

*Abbreviations*

| | |
|---|---|
| BF | bifaciality factor |
| CEE | cloud enhancement event |
| COM | component object model |
| CS | clear sky |
| DHI | diffused horizontal irradiance |
| DNI | direct normal irradiance |
| GHI | global horizontal irradiance |
| GTI | global tilted irradiance |
| HC | hosting capacity |
| LV | low-voltage |
| MPV | monofacial photovoltaic |
| OpenDSS | open distribution system simulator |
| PV | photovoltaic |
| SDG | sustainable development goal |
| TUAS | Turku University of Applied Sciences |
| VBPV | vertically mounted bifacial photovoltaic |

*Symbols*

| | |
|---|---|
| $A$ | area ($m^2$) |
| $E$ | area-specific energy* ($kWh/m^2$) or energy* (kWh) or normalized energy* (kWh/kWp) |
| $P$ | area-specific power* ($W/m^2$ or $kW/m^2$) or power* (W or kW) |
| $V$ | voltage (V) |
| $\beta$ | temperature coefficient for efficiency (%/°C) |
| $\eta_{STC}$ | standard test condition efficiency (%) |

**Table 1**
The United Nations SDGs advanced in this study and the exact contributions toward these SDGs.

| Goal | Contribution |
|---|---|
|   | PV is a clean electricity source, and its cost is decreasing, whereas electricity prices are at an all-time high. Moreover, VBPV increases the self-consumption of solar energy. Thus, promoting PV advances SDG7. |
|   | The benefits that can be achieved by expanding PV portfolio solutions beyond traditional technologies and installations require innovative and novel thinking in the PV manufacturing industry and infrastructure planning, advancing SDG9. |
|   | Increasing PV penetration in LV grids allows both cities and individual inhabitants to promote sustainable energy production. This contributes to advancing SDG11. |
|   | As a zero-carbon energy source (during use), PV contributes to decreasing greenhouse gas emissions and reaching carbon neutrality, thus advancing SDG13. |

to GTI via transposition modeling [35]. Once the GTI is known, the power output of the PV panel can be modeled based on the GTI, temperature, wind speed, and the panel's technical data.

The PV power production profile can be used as an input in power grid modeling. The effect of PV on the local power grid has been analyzed in multiple studies [8,11,16,25,32]. Voltage rise is typically the most significant during peak power production. For instance, if the voltage rise is the bottleneck factor setting a limit on the PV hosting capacity of a power grid, the conditions during the highest power production set the criteria regarding how much PV energy can be added to the grid. To increase the amount of produced PV electricity without causing severe voltage rises, it is favorable to have a PV power production profile where the amount of total production compared to peak production is high. Moreover, the temporal match between peak power production and peak electricity demand increases self-consumption and reduces the amount of PV electricity supplied to the grid, enabling even more PV production. These properties can be achieved using vertical, east–west-facing bifacial photovoltaic panels (VBPV), which produce two power peaks: morning and evening, when electricity consumption is high. Compared to conventional, equator-facing, and tilted monofacial photovoltaic panels (MPV), which produce one large peak around noon when electricity consumption is low, VBPV increases self-consumption due to a better match between production and load. For mid-latitude locations, the tradeoff between temporal production profile shift and total produced energy is reasonable even with low albedo [2]. Thus, VBPVs have a large potential for power production. The benefits of VBPV are especially clear at high-latitude locations, such as the Nordic countries, during the summer months due to low solar elevation angles and long daylight period [13]. However, applying VBPV can create additional error source to the simulation workflow: a study done in Switzerland showed that the error of modelled GTI for bifacial systems is high for steep tilt angles [21].

This study presents a comprehensive modeling chain that starts from the GHI and ends in finding the PV hosting capacity of a low-voltage (LV) power grid. The workflow is designed so that a vast number of different PV cases with varying panel locations, orientations, and technologies can be analyzed. This allows for the effective optimization of the most suitable PV portfolio for a particular power grid, considering the grid's properties, consumer load characteristics, and local solar irradiation conditions.

### 1.1. Objectives and structure of the study

This study presents a workflow for analyzing the effects of high PV penetration on an LV distribution grid, demonstrating its strengths and current development targets (e.g., load modeling and capturing local weather variations). The workflow is applied to a case study of a high-latitude location (Turku, Finland, 60.4° N, 22.3° E) to determine how much the PV hosting capacity of a test grid (IEEE European Low Voltage Test Grid) can be increased by applying VBPVs. Turku was chosen as the test location because its latitude is representative of the latitudes of the most densely populated areas in the Nordic countries. The main objective of the developed methodological workflow is to boost the PV hosting capacity of LV distribution grids in Nordic countries by coupling traditional MPV systems to VBPV.

Several Sustainable Development Goals (SDGs) set by the United Nations, especially goals 7, 9, 11, and 13, are advanced in this study. A detailed description of the contributions to the SDGs is presented in Table 1.

This work is structured as follows: Section 2 presents both the generalized workflow (Section 2.1) and the detailed methodology used in the case study (Section 2.2). Section 3 presents the key findings and results of the analyses of the different cases applied in the case study. This section is organized according to the outcomes related to the PV

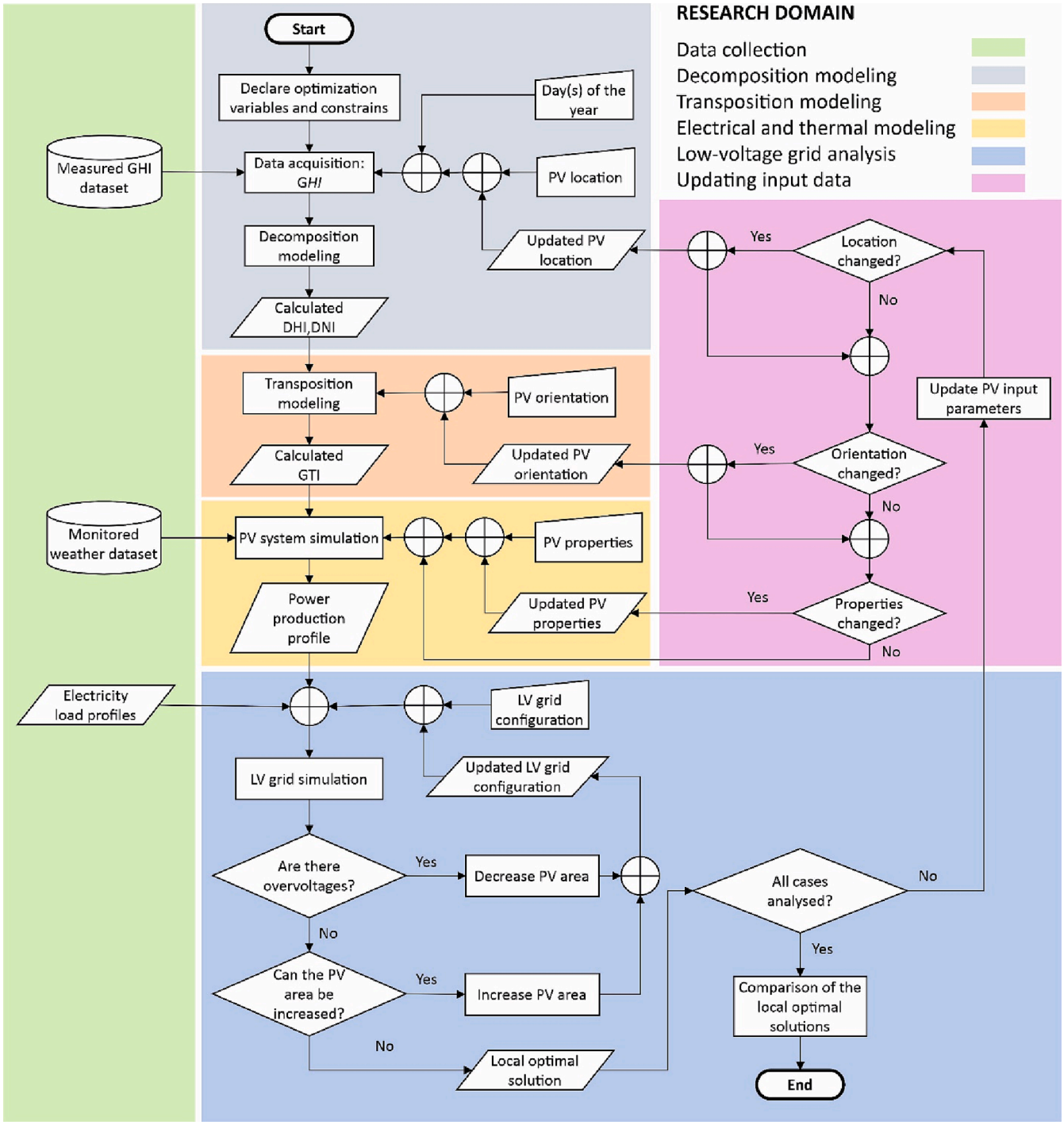


**Fig. 1.** The suggested workflow for analyzing the PV integration to the LV grid. The background colors of the different areas indicate the domain. All input datasets had a temporal resolution of one minute. The symbols used were chosen according to the ISO 9001 standard. In the case study, the workflow was applied to determine the increase in PV hosting capacity that can be achieved by utilizing VBPV systems in Nordic conditions.

power production profiles (Section 3.1), the outcomes of the LV grid simulations (Section 3.2), and a detailed analysis of one simulation with fixed electricity loads and a PV production profile (Section 3.3). Finally, Section 4 presents a short summary of the study and the main lessons learned and offers further developments and applications.

## 2. Methodology

### 2.1. Methodological workflow

The methodological workflow (Fig. 1) is arranged into five primary domains: data collection, decomposition modeling, transposition modeling, electrical and thermal modeling, and LV grid analysis.

The irradiation modeling chain (i.e., decomposition and transposition modeling) provides a calculated GTI profile for the chosen location, time, and PV orientation. The GTI is then converted to PV

electricity output, considering weather data and PV panel properties (electrical and thermal modeling). Finally, the LV grid analysis determines the maximum PV system size that can avoid overvoltage events. It is worth highlighting that the different cases are defined by changing at least one of the PV input parameters (i.e., PV location, PV properties, and PV orientation) in the electrical and thermal modeling domain. For each case, the PV system size varies in the LV grid analysis domain until sufficient resolution is found.

Once a case is analyzed, the next case is modeled and initialized depending on the research question. If only the PV panel properties are changed, the GTI profile is unaltered. Conversely, the GTI profile is recalculated when the location and/or the orientation is modified. If only panel orientation is changed, GTI can be calculated via transposition modeling (red domain in Fig. 1) using existing DNI and DHI data. However, if the panel location is changed, new DNI and DHI datasets have to be obtained, either via decomposition modeling (light blue domain in Fig. 1) or direct measurements. The finishing criteria "All cases analyzed?" = "Yes" means that LV grid simulations are done, and the optimal PV system sizes found with all PV configurations are included in the specific study.

The workflow is extremely flexible, and the model chain can be modified for application to different case studies depending on the data availability. For instance, when measured DHI and DNI values are available, the decomposition modeling domain can be skipped.

### 2.2. Methodology for the case study

#### 2.2.1. Data collection

The solar irradiance and weather data were acquired from a weather station managed by Turku University of Applied Sciences (TUAS) located in Turku, Finland. The GHI was measured by two Kipp and Zonen SP10 secondary standard pyranometers—spectrally flat Class A—and the ambient temperature and wind speed values were monitored using an Hmp110 weather transmitter. The devices transmit data using the Modbus protocol, and a single-board computer collects data every six seconds; afterwards, the data are averaged to a one-minute resolution. One-minute data is used in the following simulations to catch the highly dynamic variation of PV production due to clouds and the stochastic nature of the residential single-house electricity load profiles. Although, it should be noted that this choice may limit to compare the results directly with studies where lower temporal resolution is used.

#### 2.2.2. PV power production modeling

Two summer days to which the proposed workflow was applied were chosen: the 2nd of June (6/2) and the 1st of August (8/1) 2018. The chosen date of 6/2 represents a clear summer day close to summer solstice (three weeks' difference), whereas the 8/1 consists of a partly cloudy day with a larger temporal difference from the summer solstice. The absolute worst-case scenario in terms of voltage rise over the whole year depends, besides irradiation values, also on panel orientation, ambient temperature and electricity load. However, running the simulations with these two example days should catch the conditions that are among the most challenging ones for the LV grid. The GHI values acquired during these days were decomposed into DHI and DNI through the Starke decomposition model [27] using the coefficients for the subarctic climate zone (Dfc according to Köppen–Geiger classification) [4] where Turku is located. The PVLIB toolbox (version 1.4) for MATLAB [29] was used to support decomposition modeling.

A two-step quality control process was applied. First, all datapoints with GHI $< 50$ W/m$^2$ were excluded since decomposition modeling presents high uncertainty in low irradiance conditions [34]. Second, the quality control method proposed by Böök et al. [5] was applied to the DNI-DHI pairs.

Then, the GTI was estimated using the Perez transposition model and the binning and coefficients presented in Utrillas and Martinez-Lozano [31] for five surface orientations: south-oriented surfaces with 15°, 30°, and 40° tilt angles and vertical (90° tilt angle) east- and west-oriented surfaces. The model was implemented in MATLAB, where the PVLIB toolbox was used. Albedo was assumed to be 0.2.

The power production per PV surface unit was calculated for the MPV (south-facing with 15°, 30°, and 40° tilt angles) based on respective GTIs and panel temperatures calculated using King's model, which is also known as the "Sandia model"[17], assuming standard test condition efficiency ($\eta_{STC}$) of 18%, and the temperature coefficient ($\beta$) of −0.41 %/°C [30]. The value of $\beta$ was set to −0.41 %/°C to be consistent with [30] and to represent a real bifacial solar panel (PrismBi-60), which power production data the authors are using in other studies, such as [14] and future works. The relatively high $\beta$ and neglection to lower the module temperature by modifying the surroundings through e.g. combining PV with a green roof [3] can cause relatively high power production drop for hot and clear days. For the east–west VBPV, the power production was calculated for both the front side facing east (VBPV-E) and west (VBPV-W) cases using vertical east- and west-surface GTIs with a bifaciality factor (BF) = 90%; in other words, the additional loss of production when light was induced from the rear side was 10%. The $\eta_{STC}$ and $\beta$ coefficients were the same as for MPV. Profiles including both MPVs and VBPVs, referred to hereafter as hybrid profiles, were created by combining MPV (30° tilt) and VBPV (50:50 mixture of VBPV-E and VBPV-W) profiles with weight ratios running from 0% to 100% with a 10% step. This resulted in 15 different power production profiles for each day:

- Three MPV profiles with different tilt angles (notation: MPV-tilt, where tilt is the tilt angle in degrees).
- Three VBPV profiles (notation: VBPV-E and VBPV-W for the front side facing east and west, respectively, and VBPV for the 1:1 mixture of VPBV-E and VBPV-W).
- Nine hybrid profiles (notation: $MPV_xVBPV_{100-x}$, where $x$ is the share of the MPV area of the total system area in %).

Cloud enhancement events (CEEs) [28] can cause high and short power peaks that are problematic for the power grid. If a CEE occurs close to the peak production time, the power peak can exceed the nominal value of the panel. This can cause an overvoltage event in the power grid. These events can be mitigated in real conditions by limiting the inverter power. However, since the effect of inverters were excluded from this study, the CEE-induced power peaks that increase maximum power production were eliminated by the following filtering procedure:

1. Power production was calculated for each case using clear sky (CS) irradiance instead of modeled (GHI-based) irradiance. CS irradiance was calculated with the Ineichen–Perez model [22] in PVLIB.
2. Temporal moments when the power with CS irradiance exceeded 85% of the daily maximum value were determined.
3. For these moments, power production exceeding the CS value was curtailed.

The resulting filter effectively curtailed the CEE-induced peaks that increased the daily maximum power value, whereas the effect on power production outside of these moments was minimal. The filter is described in more detail in Appendix A.

For each profile, the maximum power production per area $P_{max,A}$ [kW$_p$/m$^2$], the total daily energy production $E_{tot,A}$ [kWh/m$^2$], and the normalized daily energy production $E_{norm}$ were determined using Eq. (1).

$$E_{norm} = \frac{E_{tot,A}}{P_{max,A}} \left[\frac{kWh}{kW_p}\right] \quad (1)$$

The methodology presented above neglects power production when GHI $< 50$ W/m$^2$. This effect was studied by analyzing measured data from a VBPV at the same location with a one-minute resolution [23]. The daily total power output of the panel on 6/2 and 8/1 was calculated

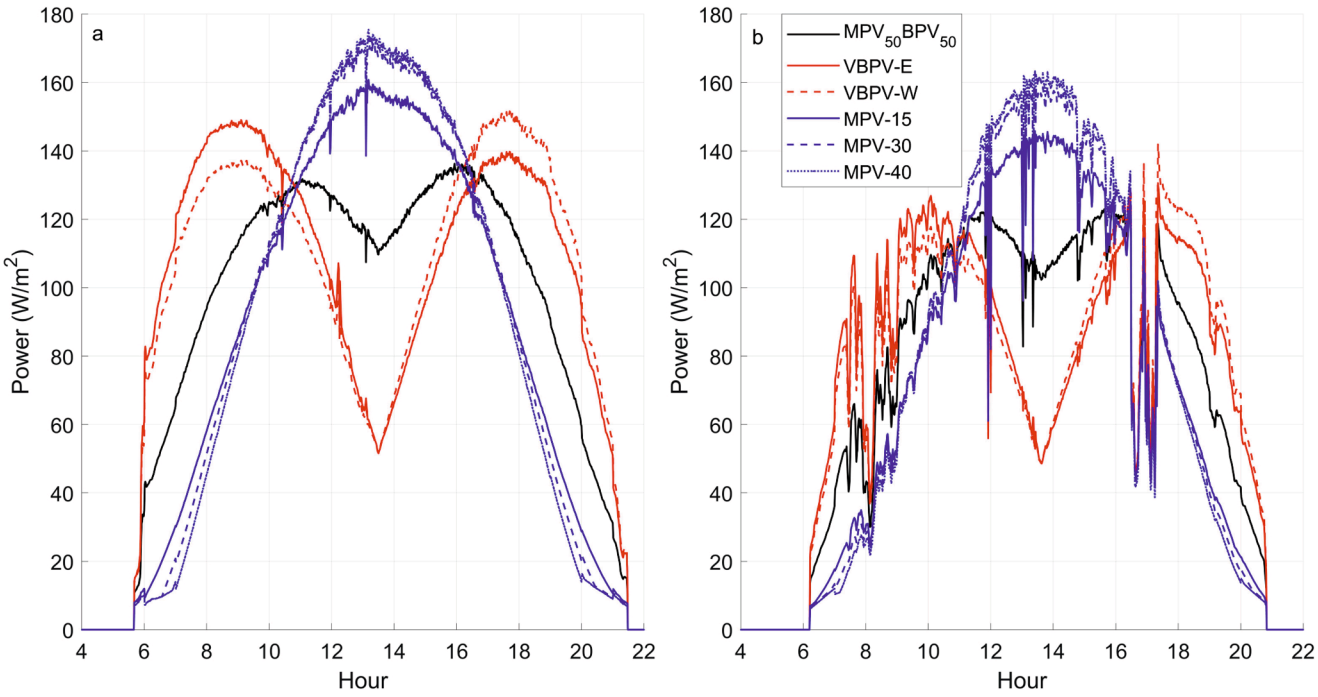


**Fig. 2.** Modeled power production of VBPV-W, VBPV-E, and MPV with 15°, 30°, and 40° tilt angles and hybrid profiles combining VBPV and MPV-30 profiles for (a) 6/2 and (b) 8/1.

separately by including all measured data points and by including only those measured data points when the measured GHI at the same time was at least 50 W/m$^2$. The latter approach underestimated the daily PV production by up to 1.1%, which was considered reasonable since this is small compared to the differences between the MPV and VBPV hosting capacities.

### 2.2.3. Low-voltage grid modeling

The IEEE European Low Voltage Test Grid [26] was used as the test network. The grid was simulated in the Open Distribution System Simulator (OpenDSS, version 9.4.1.1) [9], controlled by MATLAB via the COM interface. The GridPV toolbox for MATLAB (version 2.2) [6] was utilized to control OpenDSS. OpenDSS has been widely used to analyze the grid effects of distributed power generation [10,20,24,33]. The network presents a typical small European neighborhood distribution grid with 55 residential single houses as loads. The distribution grid is connected to the main grid via an 11 kV/416 V substation. Voltage limits were set to 0.9–1.1 per unit (p.u.) according to the EN 50160 standard [19], meaning that ± 10% deviation from the nominal value was accepted.

The one-minute resolution load profiles were taken from the databank provided with the text grid, which contained 100 load profiles. Forty different load location cases were prepared by randomizing the load profiles used for each consumer 40 times (each load profile was allowed to exist only once per case). Two different load size cases, "low" and "high", corresponding to 8–8.5 and 16–17 kWh/consumer during one day, respectively, were used, resulting in 80 different load cases.

For each load case (location / size), the analysis of voltage drops in the grid was done first without PV by varying the substation voltage ($V_{sub}$) with 0.005 p.u. resolution until the minimum value that could still avoid lower voltage limit violations during the day was found. This value was set to $V_{sub}$ during the entire day; $V_{sub}$ is assumed to be controllable, so it can be changed once per day. Then, PV systems were added to each house according to the given profile, and the maximum PV power that avoided upper voltage limit violations was determined using the following algorithm:

1. The profile was scaled so that the peak production $P_{max}$ = 0.5 kW. The first simulation was run to check the upper voltage limit (1.1 p.u.) was not violated.
2. The $P_{max}$ was doubled, and the simulation was repeated with the new $P_{max}$ until the upper voltage limit was violated.
3. The $P_{max}$ was set halfway between the highest successful (no $V$ violations) and lowest failed ($V$ violations) values, and the simulation was repeated. This was repeated until the defined resolution (0.125 kW) was reached.
4. The highest $P_{max}$ value that avoided $V$ violations was chosen as the maximum PV peak capacity.

The total power production ($E_{tot}$), the area of the system ($A$), and the PV hosting capacity ($HC_{PV}$) were calculated according to Eqs. (2)–(4).

$$E_{tot} = P_{max} \bullet E_{norm} \tag{2}$$

$$A = \frac{P_{max}}{P_{max,A}} \tag{3}$$

$$HC_{PV} = \frac{E_{tot} \bullet n}{E_{cons}} \tag{4}$$

where $n$ is the number of PV systems in the grid, and $E_{cons}$ is the total daily electricity consumption.

### 2.2.4. Limitations of the methodology

The methodology presented above focuses on enabling the rapid analysis of different PV cases and comparing them. The focus of the case study was to analyze the effect of VBPV on a grid's PV hosting capacity, and to allow rapid analysis to guide further, more detailed research, simplifications were made. Most importantly, the load profiles used were synthetic and delivered with the test grid code, and the effect of seasonal variations in electricity consumption was omitted. However, since the focus of the case study was to analyze the effects of the PV production profile shape on the hosting capacity, this simplification was considered reasonable. The hosting capacity of the power grid was determined solely by the voltage rise. Although this is a common case

**Table 2**
The key statistical factors of the shown PV power output profiles were maximum power during the day, total daily energy production, and normalized energy production (the fraction of energy production and maximum power).

| Day | PV profile | $P_{max,A}$ (W/m$^2$) | $E_{tot,A}$ (kWh/m$^2$) | $E_{norm}$ (kWh/kW$_p$) |
|---|---|---|---|---|
| 6/2 | VBPV-E | 149 | 1.71 | 11.45 |
| | VBPV-W | 152 | 1.70 | 11.23 |
| | MPV-15 | 161 | 1.47 | 9.13 |
| | MPV-30 | 173 | 1.49 | 8.63 |
| | MPV-40 | 175 | 1.47 | 8.38 |
| | $MPV_{50}VBPV_{50}$ | 136 | 1.59 | 11.71 |
| 8/1 | VBPV-E | 131 | 1.27 | 9.75 |
| | VBPV-W | 142 | 1.27 | 8.96 |
| | MPV-15 | 146 | 1.18 | 8.10 |
| | MPV-30 | 159 | 1.23 | 7.74 |
| | MPV-40 | 163 | 1.23 | 7.55 |
| | $MPV_{50}VBPV_{50}$ | 125 | 1.25 | 10.03 |

[12], in some cases, other factors, such as transformer capacity or harmonic currents [15], could set stricter limits to PV penetration.

To perform analysis relevant to full-year operation with only two example days, the day 6/2 was chosen since it was almost completely sunny day close to summer solstice and thus it is reasonable to expect that the observed peak PV production during that day is close to real annual maximum. Respectively, 8/1 represents a summer day with varying weather, and hence it allows to analyze the effects of rapid fluctuation of PV production. Thus, these days are expected to be among the most difficult ones for the LV grid and it is expected that if the PV system is sized based on these example days, the potential voltage violations during other days can be prevented by minor curtailment. Since both example days were summer days, the conditions for PV production were far better than during the other seasons. Thus, PV penetration, calculated as a fraction of annual electricity production and consumption, was significantly smaller than the daily values calculated here. In the case study, these simplifications were considered acceptable since the key result, the effect of adding VBPV to the system, could be extracted. Moreover, PV production was calculated in ideal surroundings (no shading from adjacent panels, trees, or buildings). This overestimated PV production compared to real installations, but in a comparative study, the main interest was the relative power production in different cases.

In this case study, all of the simplifications described above were considered reasonable, and the presented results are valid. When the workflow is applied to other case studies, the importance of recognizing and considering these limitations should be highlighted, and if necessary, the methodology can be developed further by, for example, using measured load profiles or setting criteria other than overvoltage to unacceptable PV production levels.

## 3. Results and discussion

### 3.1. Analysis of PV production profiles

The PV power production profiles used, MPV with different tilt angles (15°, 30°, and 40°), VBPV-E, VBPV-W, and $MPV_{50}VBPV_{50}$, are presented in Fig. 2. On 6/2 (Fig. 2a) with clear conditions, all MPV configurations produced one large power peak at solar noon (after 1 p.m.: 175 W/m$^2$ for MPV-40 and MPV-30 and 160 W/m$^2$ for MPV-15), whereas VBPV-W and VBPV-E produced lower power peaks (135–150 W/m$^2$) at 9 a.m. and 6 p.m. For VBPV, the peak was higher at around 15 W/m$^2$ when the direct irradiance was on the front side due to additional optical losses with rear-side irradiance. Similar behavior was observed with both measured and modelled data from a green-roof VBPV and MPV panels in Switzerland [2], although the particular VBPV system azimuth is deviating from E-W orientation by 25°, resulting as high morning and low evening PV peak production. Moreover, the results shown in Fig. 2 are in line with another set of simulation of a clear summer day VBPV production in Turku (Finland), which was validated against measured data [14].

Finally, for the hybrid case $MPV_{50}VBPV_{50}$, the power peaks were lower than in pure VBPV cases, and they were shifted toward noon, from 9 a.m. to 11 a.m., and from 6 p.m. to 4 p.m. Therefore, it is worth noting that the power peaks were closer to each other, and the match with the typical daily profile of energy consumption decreased (i.e., the need for alternative energy production early in the morning and late in the afternoon was increased). However, the relatively smooth profile between 8 a.m. and 7 p.m. was grid friendly and allowed high total production compared to peak production.

The same trends were observed on 8/1 (Fig. 2b), which featured partly clear and partly cloudy conditions. The general shapes of the profiles were similar to the 6/2 case, but the profiles were more unstable, with multiple sharp peaks and valleys due to variable weather conditions throughout the day. In general, as expected, the peak values were lower for all the peaks (by 12–18%), even for the clear periods, due to the longer temporal difference to summer solstice. Moreover, the length of the daylight period was slightly shorter on 8/1 than on 6/2, which can be seen from Fig. 2. This is due to the increased temporal difference between the example day and summer solstice.

Table 2 shows the key statistical parameters describing the profiles shown in Fig. 2: the maximum power per area ($P_{max,A}$) and the total produced electricity per area ($E_{tot,A}$) during the daily simulations and the normalized energy production, which is defined as $E_{norm} = E_{tot,A}/P_{max,A}$. $E_{norm}$ describes the smoothness of the profile: high $E_{norm}$ indicates relatively smooth power production, whereas low $E_{norm}$ is typical for a profile with high peak and low off-peak production. Since overvoltage events typically occur near peak production, the $P_{max,A}$ of the system is likely to set the limit for the PV hosting capacity; thus, profiles with high $E_{norm}$ are expected to deliver high daily production.

The VBPV and hybrid profiles $MPV_{50}VBPV_{50}$ had significantly higher $E_{norm}$ than any of the MPV profiles due to higher overall production and lower peaks. Regarding the data from 8/1, the difference between the VBPV-E and VBPV-W profiles was significant due to a cloudy moment around the evening peak. The power peak due to a CEE occurring on 6/2 around noon can be seen from the VBPV profiles, but from the MPV and the hybrid $MPV_{50}VBPV_{50}$ profiles, it was curtailed out—in other words, the power production was limited to the calculated CS value (see Appendix A). Without curtailing, this CEE would have caused a high peak on those profiles, limiting the amount of PV energy in the grid. When comparing MPV profiles, it can be noted that MPV with a 15° tilt had a significantly lower noon peak than other MPV profiles, leading to higher $E_{norm}$, but at the cost of lower total energy production.

The effect of the share of VBPV (as a fraction of the total system area) to the shape of the hybrid profile is visualized in Fig. 3. The pure MPV profile (blue dashed line) has a high and narrow peak at solar noon. When the VBPV share is increased, the peak first starts to flatten and widen and then splits into two peaks. When the VBPV share is increased even further, the two peaks move further away from solar noon and start to rise again (when the VBPV share exceeds 40%) until the pure VBPV profile is reached. For 6/2, the changes in profile are distinct in Fig. 3a, while for 8/1, the changes in the features are partly overwritten by the weather variation, which induced peaks and valleys (Fig. 3b). However, the general shapes of the curves are visible in Fig. 3b as well. The key parameters of the profiles are shown in Appendix B (Table A2). It should be noted that the notation $MPV_{100}VBPV_0$ in Table A2 is synonymous with the notation MPV-30 in Table 2.

### 3.2. Low-voltage grid simulations

The simulations were done for both example days according to the procedure described in Section 2.2.3. The key results are summarized in Table 3. Each row shows the median values among the 40 studied load location cases (see Section 2.2.3) with the corresponding day, load size, and PV profile. For simplicity, only one out of nine hybrid profiles, the

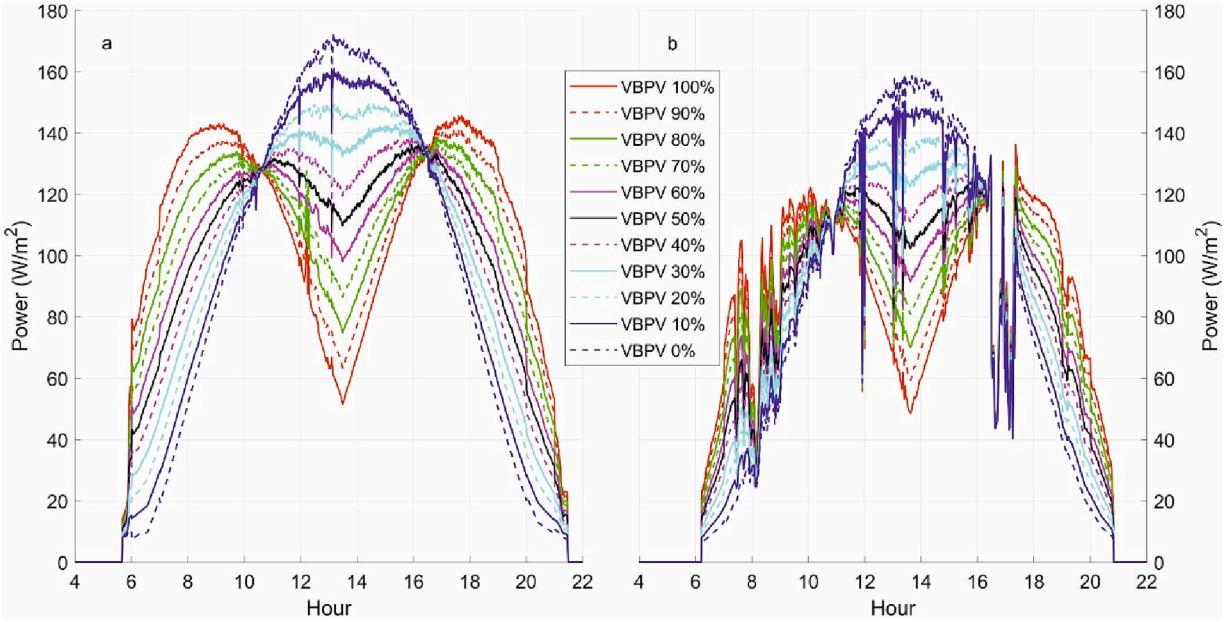


**Fig. 3.** The hybrid profiles used in this study as a function of VBPV share (% of the total system area) for (a) 6/2 and (b) 8/1.

**Table 3**
The key statistics (medians among the 40 load location cases) of the PV systems that allow maximum energy production; $E_{prod}$ is the total electricity production of one system, $E_{prod,norm}$ is the total production normalized to MPV-30, A is the system area, $A_{norm}$ is the system area normalized to MPV-30, and $HC_{PV}$ is the PV penetration level. Only one hybrid profile (one that maximizes PV production) is shown.

| Day | Load sizes | PV profile | $E_{prod}$ (kWh) | $E_{prod,norm}$ | A ($m^2$) | $A_{norm}$ | $HC_{PV}$ |
|---|---|---|---|---|---|---|---|
| 6/2 | Low | VBPV-E | 75.9 | 1.33 | 44.5 | 1.16 | 8.96 |
| | | VBPV-W | 77.2 | 1.35 | 45.4 | 1.18 | 9.05 |
| | | MPV-15 | 60.5 | 1.06 | 41.2 | 1.07 | 7.16 |
| | | MPV-30 | 57.2 | 1.00 | 38.3 | 1.00 | 6.79 |
| | | MPV-40 | 56.0 | 0.98 | 38.1 | 0.99 | 6.60 |
| | | $MPV_{30}VBPV_{70}$ | 81.0 | 1.42 | 49.4 | 1.29 | 9.53 |
| | High | VBPV-E | 43.7 | 1.35 | 25.6 | 1.18 | 2.52 |
| | | VBPV-W | 46.3 | 1.43 | 27.2 | 1.25 | 2.68 |
| | | MPV-15 | 34.2 | 1.06 | 23.3 | 1.07 | 2.04 |
| | | MPV-30 | 32.4 | 1.00 | 21.7 | 1.00 | 1.93 |
| | | MPV-40 | 31.4 | 0.97 | 21.4 | 0.98 | 1.89 |
| | | $MPV_{30}VBPV_{70}$ | 47.2 | 1.46 | 28.8 | 1.33 | 2.74 |
| 8/1 | Low | VBPV-E | 67.1 | 1.31 | 52.6 | 1.27 | 7.81 |
| | | VBPV-W | 62.8 | 1.22 | 49.3 | 1.19 | 7.35 |
| | | MPV-15 | 53.7 | 1.05 | 45.4 | 1.09 | 6.32 |
| | | MPV-30 | 51.3 | 1.00 | 41.6 | 1.00 | 6.05 |
| | | MPV-40 | 50.0 | 0.98 | 40.6 | 0.98 | 5.90 |
| | | $MPV_{30}VBPV_{70}$ | 68.8 | 1.34 | 54.7 | 1.31 | 7.97 |
| | High | VBPV-E | 40.2 | 1.36 | 31.6 | 1.32 | 2.40 |
| | | VBPV-W | 40.3 | 1.37 | 31.7 | 1.32 | 2.34 |
| | | MPV-15 | 30.9 | 1.05 | 26.1 | 1.09 | 1.83 |
| | | MPV-30 | 29.5 | 1.00 | 23.9 | 1.00 | 1.75 |
| | | MPV-40 | 28.8 | 0.98 | 23.3 | 0.98 | 1.70 |
| | | $MPV_{20}VBPV_{80}$ | 42.2 | 1.43 | 33.4 | 1.39 | 2.48 |

one that allows the highest PV production for the particular day/load size combination, is shown in Table 3. The identical table for the rest of the hybrid profiles is included in Appendix C (Table A3).

For all day / PV profile -combinations, the total daily PV electricity production ($E_{prod}$) was higher with the "low" load case than with the "high" load case. This is due to the assumptions related to the controllability of the substation voltage (Section 2.2.3). Since the $V_{stub}$ remains constant through the day, higher loads force higher value for $V_{stub}$ to avoid the lower voltage limit violations, leaving less space for voltage rise due to PV overproduction. This effect is stronger than the possibility to produce additional electricity from PV for self-consumption with higher loads. The VBPV profiles give a significant production boost between 22% (VBPV-W on 8/1 with low load sizes) and 43% (VBPV-W on 6/2 with high load sizes) due to both increased system size and higher production per unit area compared to the reference case (MPV-30). For each VBPV case, both production and the system area were increased, and the increase was higher for production. Mixing MPV and VBPV with an optimal ratio (to maximize energy production) increased production and system size even further: the highest production increase was 46%, achieved on 6/2 with high load sizes and the $MPV_{30}VBPV_{70}$ profile. This was due to the smoother profile shape (i.e., higher total/peak production ratio) and improved match with the electricity load. The optimal hybrid profiles were strongly weighted to VBPV (typically 70 %) (Fig. 4). Tilted MPV can be easily installed on roofs, but finding suitable locations for VBPV in household-level installations might be challenging, although creative architectural thinking enables novel solutions to facilitate VBPV installations [13,18]. Moreover, if the VBPV share is increased more than the location allows, shading between the adjacent rows reduces production. Therefore, it is realistic to think that hybrid systems may be more weighted toward MPV installations. However, even a small number (10–30%) of VBPVs can give a reasonable production boost to the system (Fig. 4), and 40% of VBPVs already gives rather similar results in terms of total energy production compared to the optimal 70%. However, the temporal location of the peaks depends on the VBPV share: with low VBPV shares, the peaks are closer to solar noon, and the benefit of matching production and load is at least partly lost.

In the simulations shown here, especially with low load sizes, PV production was very high compared to energy consumption. This is due to the small geographical area covered by the grid, resulting in a short distance to the substation and low voltage losses in power lines, and the assumption that all the produced excess PV electricity can be delivered to the main grid. Therefore, the results presented here are likely to overestimate the absolute values of the PV hosting capacities of grids compared to most of the real European distribution feeders. However, the main interests of this study in developing a comprehensive methodological workflow are twofold: (i) to demonstrate the difference between MPV and VBPV configuration systems, and (ii) to boost the hosting capacity in distribution LV grids with VBPV in Nordic conditions. The significant overproduction highlights that the optimal system

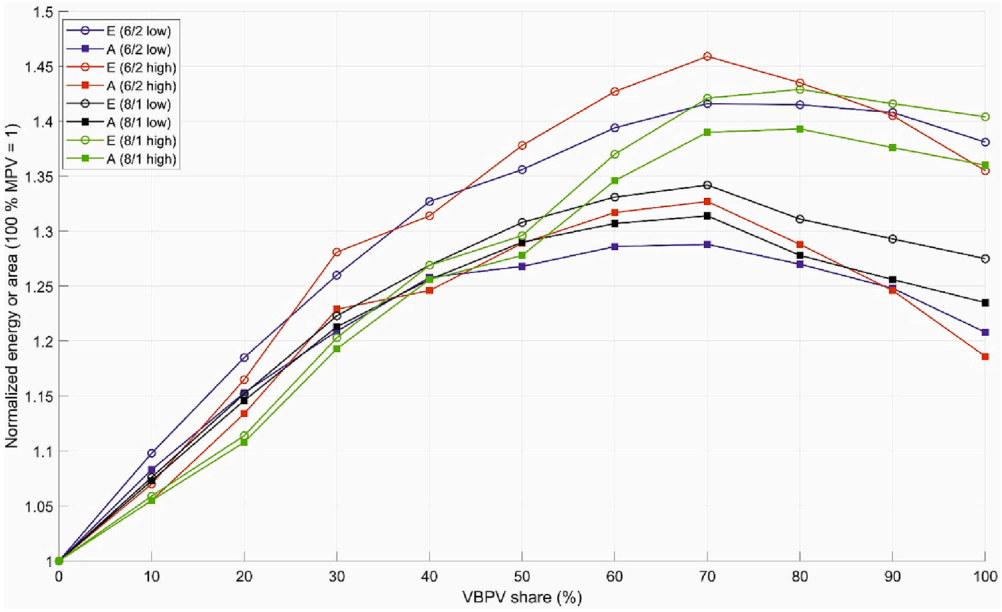


**Fig. 4.** The relative increase (compared to MPV with a 30° tilt) of the produced energy (E) and system area (A) with the hybrid profiles. The colors indicate the day and load size cases.

for practical application may not be the one that maximizes production: load-match design [1] may be a more useful solution. This would mean that some of the suitable MPV installation sites are left unused to avoid high overproduction at noon.

The largest allowed PV system area was larger in every case when data from 8/1 were used. This was expected because less optimal irradiation conditions allowed more PV energy in the grid without exceeding the hosting capacity. In reality, the area of the PV system is not varied, so the maximum allowed capacity should be determined based on the optimal PV production conditions (clear summer solstice day) or on close-to-optimal conditions, such as the real 6/2 GHI data presented here. In the latter case, curtailment may be needed closer to summer solstice to avoid overvoltage events.

### 3.3. In-depth analysis of one example simulation

To clarify the procedure, a detailed example of simulating one individual case is presented in this section. The presented case used the solar irradiation data from 6/2, the high-load-size case, one load location case (see Section 2.2.3), and the optimal PV production profile for that particular case ($MPV_{30}VBPV_{70}$). The selected location case was chosen because its PV production was the closest to the median with the $MPV_{30}VBPV_{70}$ profile and high load sizes, and it did not have a significant difference from the median in any case. The difference between the chosen load location case and the median of all 40 cases was 0–4.9% (average 1.5%) when all day/load size/hybrid PV profile combinations were considered.

#### 3.3.1. Analysis of the grid without PV

The smallest allowed $V_{sub}$ was determined according to the procedure described in Section 2.2.3. In this case, $V_{sub}$ = 1.020 p.u. Fig. 5a shows the power consumption, and Fig. 5b shows the observed minimum and maximum voltages in the network as a function of time for $V_{sub}$ = 1.020 p.u. The lowest voltage occurred simultaneously with the highest demand at 8:05 p.m.

Fig. 5c–h show snapshot images of the test grid during the day divided into night (c), morning (d), early (e) and late (f) afternoon, the peak electricity load (g), and late evening (h). The exact moments for d–f were chosen due to interesting behavior with PV (discussed in Section 3.3.2), but the same times were used to enable easy comparison between the cases without and with PV (see Section 2.2.3). The snapshots show that the voltage drop in the grid was connected to electricity demand: high demand requires high currents, leading to high losses. It should be noted that the minimum voltage shown in Fig. 5b is the minimum among all phases, whereas the snapshots show the average voltage of different phases for each node; thus, the values shown in the snapshots are well above the actual lower limit.

#### 3.3.2. Analysis with PV

The PV hybrid systems ($MPV_{30}VBPV_{70}$) were added to each house (load) connected to the grid, and the highest allowed peak power was determined as described in Section 2.2.3. For this example, $P_{max}$ = 4 kW. The net load (electricity load – PV production) is shown in Fig. 6a, and the minimum and maximum voltages are shown in Fig. 6b as a function of time. The snapshot images of the network are shown in Fig. 6c–h to visualize voltage behavior and differences in it during the night (c), PV morning peak and peak voltage time (d), PV noon valley (e), PV evening peak (f), the moment of maximum electricity consumption (g), and late evening (h).

Since the PV production capacity exceeds daily electricity consumption (by a factor of 2.88 in the case shown here), the net load shown in Fig. 6a is negative during the daytime: the grid is producing more electricity than it consumes, and the current flows in a reversed direction. Fig. 6b shows that the high voltage values (>1.05 p.u.) are measured almost continuously from 6 a.m. to 8 p.m. due to high PV production. This can be explained by the relatively flat PV production profile achieved with $MPV_{30}VBPV_{70}$.

The snapshots (Fig. 6c–h) show high voltages around the grid when PV production is high (d–f). For (g), reasonably high PV production is consumed by peaking electricity demand, resulting in lower voltages. Interestingly, the voltage peak (in any phase) was achieved at 8:30 a.m., although the average voltage of all phases was significantly higher at 4 p.m., which can be seen by comparing (d) and (f). This is likely due to a sharp demand peak in one phase at 8:30 a.m. (Fig. 5a), which causes a voltage drop in the phase in which the peaking load is connected and a voltage rise in other phases at the location of the peaking load (Fig. 5b and 6b). At 4 p.m., the demand is relatively flat (Fig. 5a), and the voltage is high all over the grid. This highlights that the limiting factor for PV penetration using the methodology presented in Section 2 is related to the sharp peaks in the load and PV production profiles. The sharp peaks

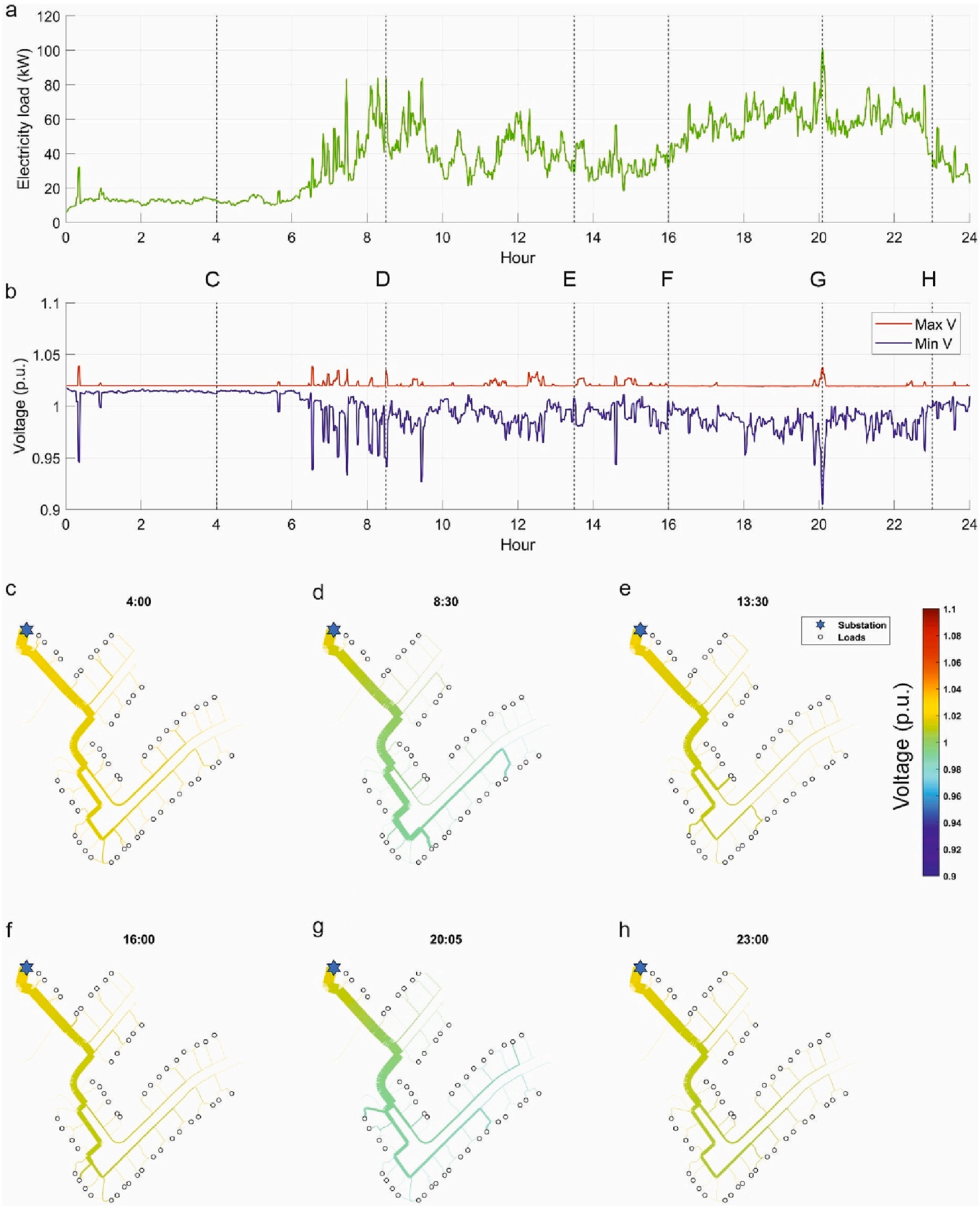


**Fig. 5.** (a) The total electricity load (measured from the substation) of the grid studied (IEEE European Low Voltage Test Grid, 55 residential single houses as loads) and (b) the minimum and maximum observed voltages as a function of time without any PV production. Snapshot images of the grid at different times (c–h) showing the voltage variations during the daily simulation. The color in c–h shows the voltage (average of all phases) in each node, whereas the line thickness shows the current normalized to the maximum current at the given moment. The capital letters C–H and the black vertical dashed lines in (a) and (b) show the moments when the snapshots were taken.

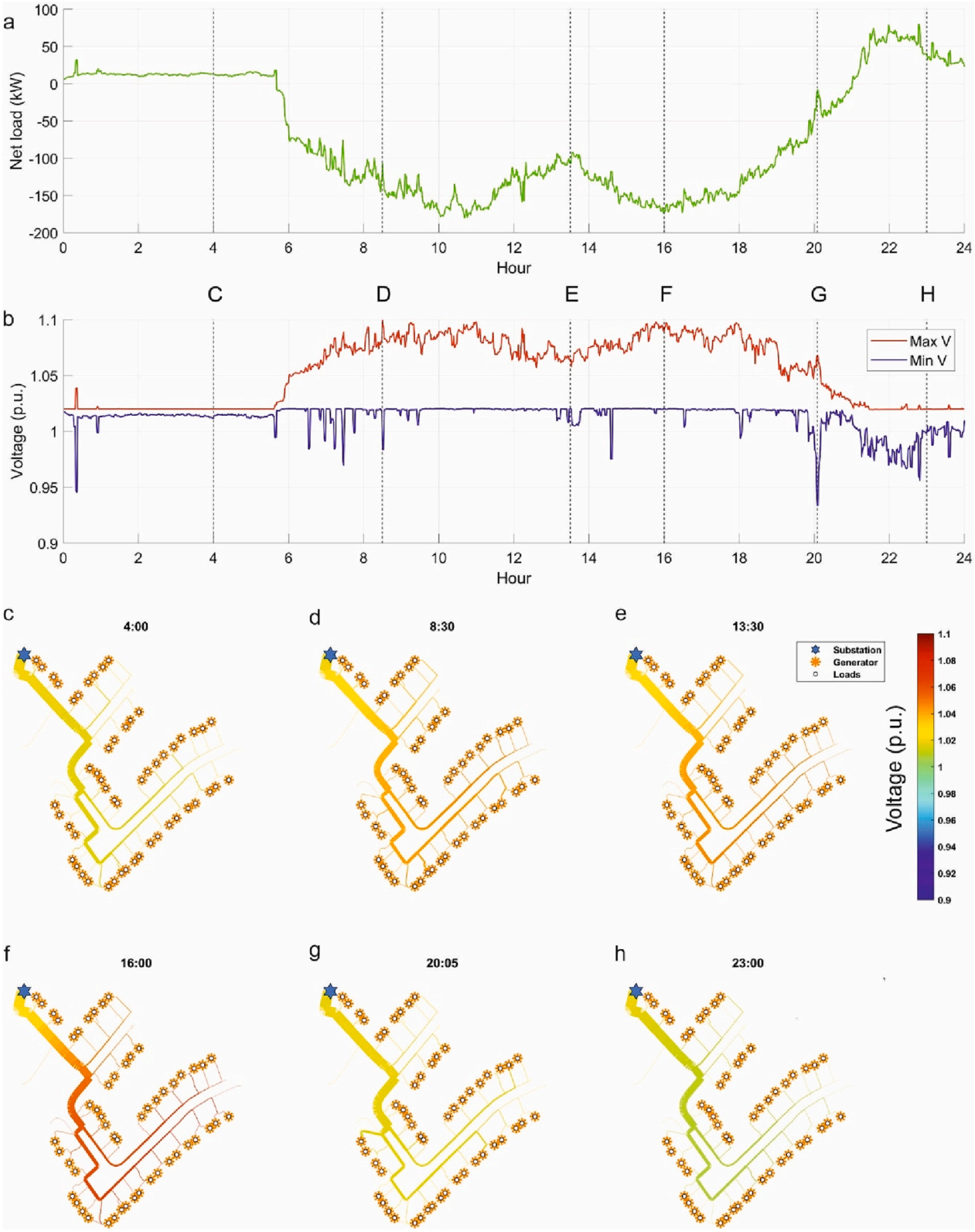


**Fig. 6.** (a) The total electricity net load (measured from the substation) of the grid studied (IEEE European Low Voltage Test Grid, 55 residential single houses as loads) and (b) the minimum and maximum observed voltages as a function of time with the $MPV_{30}VBPV_{70}$ PV profile. Snapshot images of the test grid at different times (c–h) showing the voltage variations during the daily simulation. The colors in c–h show the voltage (average of all phases) in each node, whereas the line thickness shows the current normalized to the maximum current at the given moment. The capital letters C–H and the black vertical dashed lines in (a) and (b) show the moments when the snapshots were taken.

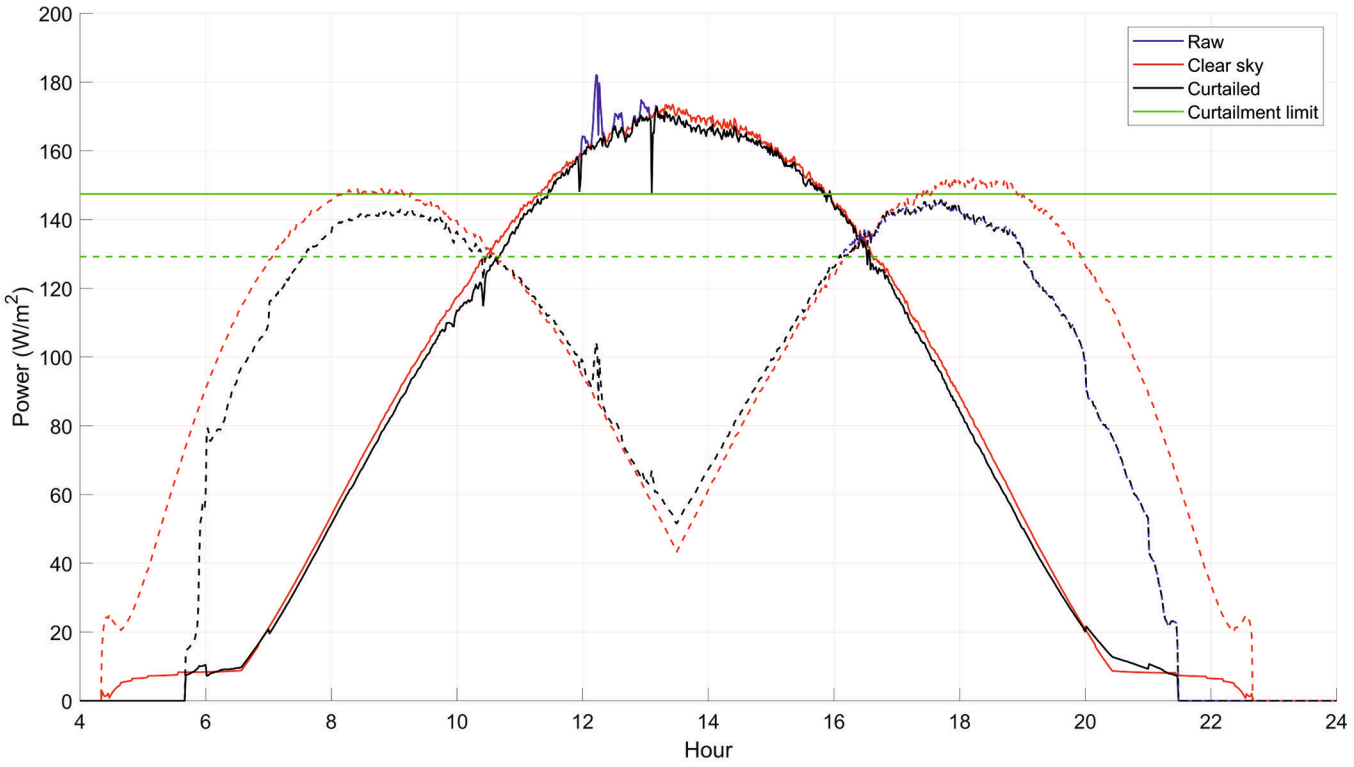


**Fig. A1.** The effect of the applied curtailment method on 6/2 for MPV-30 (solid lines) and VBPV (dashed lines).

**Table A1**
The key parameters describing the raw and curtailed power profiles.

| PV type | Parameter (unit) | Raw profile | Curtailed profile | Relative change (%) |
|---|---|---|---|---|
| MPV-30 | $P_{max,A}$ (W/m$^2$) | 182 | 173 | −5.1 |
| | $E_{tot,A}$ (kWh/m$^2$) | 1.50 | 1.49 | −0.2 |
| | $E_{norm}$ (kWh/kWp) | 8.21 | 8.63 | 5.1 |
| VBPV | $P_{max,A}$ (W/m$^2$) | 146 | 146 | 0.0 |
| | $E_{tot,A}$ (kWh/m$^2$) | 1.70 | 1.70 | 0.0 |
| | $E_{norm}$ (kWh/kWp) | 11.70 | 11.70 | 0.0 |

**Table A2**
The key parameters of the hybrid profiles, presented with same notations as in Table 2.

| Day | PV profile | $P_{max,A}$ (W/m$^2$) | $E_{tot,A}$ (kWh/m$^2$) | $E_{norm}$ (kWh/kW$_p$) |
|---|---|---|---|---|
| 6/2 | $MPV_0VBPV_{100}$ | 146 | 1.70 | 11.70 |
| | $MPV_{10}VBPV_{90}$ | 141 | 1.68 | 11.93 |
| | $MPV_{20}VBPV_{80}$ | 139 | 1.66 | 11.99 |
| | $MPV_{30}VBPV_{70}$ | 137 | 1.64 | 12.00 |
| | $MPV_{40}VBPV_{60}$ | 136 | 1.62 | 11.92 |
| | $MPV_{50}VBPV_{50}$ | 136 | 1.59 | 11.71 |
| | $MPV_{60}VBPV_{40}$ | 139 | 1.57 | 11.35 |
| | $MPV_{70}VBPV_{30}$ | 143 | 1.55 | 10.88 |
| | $MPV_{80}VBPV_{20}$ | 150 | 1.53 | 10.23 |
| | $MPV_{90}VBPV_{10}$ | 161 | 1.51 | 9.40 |
| | $MPV_{100}VBPV_0$ | 173 | 1.49 | 8.63 |
| 8/1 | $MPV_0VBPV_{100}$ | 136 | 1.27 | 9.34 |
| | $MPV_{10}VBPV_{90}$ | 133 | 1.27 | 9.56 |
| | $MPV_{20}VBPV_{80}$ | 129 | 1.26 | 9.78 |
| | $MPV_{30}VBPV_{70}$ | 126 | 1.26 | 10.01 |
| | $MPV_{40}VBPV_{60}$ | 124 | 1.26 | 10.11 |
| | $MPV_{50}VBPV_{50}$ | 125 | 1.25 | 10.03 |
| | $MPV_{60}VBPV_{40}$ | 127 | 1.25 | 9.82 |
| | $MPV_{70}VBPV_{30}$ | 131 | 1.24 | 9.47 |
| | $MPV_{80}VBPV_{20}$ | 139 | 1.24 | 8.92 |
| | $MPV_{90}VBPV_{10}$ | 148 | 1.24 | 8.33 |
| | $MPV_{100}VBPV_0$ | 159 | 1.23 | 7.74 |

can be even more problematic when considering acceptable limits to the voltage unbalance between the phases, which was excluded here. However, in power systems where all the loads have three-phase connections, these issues are easier to manage.

Finally, the results presented here can be compared to some extend with alike study done by measuring load flows and voltages at the critical points of a real LV-grid with high PV penetration, located in Germany [7]. The particular grid had oversized PV production compared to its consumption: maximum power flows during a six-week measurement period at the transformer were 150 kW and −423 kW with a total energy balance of −45 MWh, negative sign indicating situation where the LV-grid is supplying electricity to the transformer. For a clear day, [7] observed a short upper voltage limit (1.1 p.u.) violation. Active power curtailment (70% ratio) combined with reactive power control, both included to the operation of the PV inverter, reduced the relative voltage rise by 3%, providing a way to reduce voltage rise due to overproduction or CEEs with reasonable economic cost. Results from [7] validate that such surplus PV production inside an LV-grid is possible in real conditions, increasing credibility of our work and supporting our results of the potential of VBPV when maximizing the PV hosting capacity of the grid. Moreover, [7] reported that other power quality issues beside the voltage rise were in line with the EN 50160 standard.

## 4. Conclusions and further development

This study presented a comprehensive methodological workflow to boost PV hosting capacity in LV distribution grids in Nordic conditions by utilizing VBPV. Such a methodological workflow allows for the study of the effect of distributed PV on the LV grid by rapidly comparing different cases for MPV and VBPV. The workflow was designed to be flexible; the methodology can be easily adjusted based on the available data to address related research questions. This allowed us to effectively analyze the effect of any variable, such as PV production profile,

**Table A3**
The key statistics for the hybrid PV systems, using same notation than in Table 3. The data included also to Table 3 is bolded. Notation "$MPV_{100}VBPV_0$" here equals to notation "MPV-30" in Table 3.

| Day | Load sizes | PV profile | $E_{prod}$ (kWh) | $E_{prod,norm}$ | $A$ ($m^2$) | $A_{norm}$ | $HC_{PV}$ |
|---|---|---|---|---|---|---|---|
| 6/2 | Low | $MPV_0VBPV_{100}$ | 79.0 | 1.38 | 46.3 | 1.21 | 9.21 |
| | | $MPV_{10}VBPV_{90}$ | 80.6 | 1.41 | 47.8 | 1.25 | 9.36 |
| | | $MPV_{20}VBPV_{80}$ | 80.9 | 1.41 | 48.7 | 1.27 | 9.52 |
| | | **$MPV_{30}VBPV_{70}$** | **81.0** | **1.42** | **49.4** | **1.29** | **9.53** |
| | | $MPV_{40}VBPV_{60}$ | 79.7 | 1.39 | 49.3 | 1.29 | 9.40 |
| | | $MPV_{50}VBPV_{50}$ | 77.6 | 1.36 | 48.6 | 1.27 | 9.15 |
| | | $MPV_{60}VBPV_{40}$ | 75.9 | 1.33 | 48.2 | 1.26 | 8.75 |
| | | $MPV_{70}VBPV_{30}$ | 72.1 | 1.26 | 46.4 | 1.21 | 8.41 |
| | | $MPV_{80}VBPV_{20}$ | 67.8 | 1.19 | 44.2 | 1.15 | 7.89 |
| | | $MPV_{90}VBPV_{10}$ | 62.8 | 1.10 | 41.5 | 1.08 | 7.35 |
| | | **$MPV_{100}VBPV_0$** | **57.2** | **1.00** | **38.3** | **1.00** | **6.79** |
| | High | $MPV_0VBPV_{100}$ | 43.9 | 1.35 | 25.7 | 1.19 | 2.61 |
| | | $MPV_{10}VBPV_{90}$ | 45.5 | 1.41 | 27.0 | 1.25 | 2.70 |
| | | $MPV_{20}VBPV_{80}$ | 46.5 | 1.43 | 28.0 | 1.29 | 2.76 |
| | | **$MPV_{30}VBPV_{70}$** | **47.2** | **1.46** | **28.8** | **1.33** | **2.74** |
| | | $MPV_{40}VBPV_{60}$ | 46.2 | 1.43 | 28.6 | 1.32 | 2.76 |
| | | $MPV_{50}VBPV_{50}$ | 44.6 | 1.38 | 28.0 | 1.29 | 2.60 |
| | | $MPV_{60}VBPV_{40}$ | 42.6 | 1.31 | 27.0 | 1.25 | 2.48 |
| | | $MPV_{70}VBPV_{30}$ | 41.5 | 1.28 | 26.7 | 1.23 | 2.42 |
| | | $MPV_{80}VBPV_{20}$ | 37.7 | 1.17 | 24.6 | 1.13 | 2.24 |
| | | $MPV_{90}VBPV_{10}$ | 34.6 | 1.07 | 22.9 | 1.06 | 2.10 |
| | | **$MPV_{100}VBPV_0$** | **32.4** | **1.00** | **21.7** | **1.00** | **1.93** |
| 8/1 | Low | $MPV_0VBPV_{100}$ | 65.4 | 1.27 | 51.4 | 1.23 | 7.66 |
| | | $MPV_{10}VBPV_{90}$ | 66.3 | 1.29 | 52.3 | 1.26 | 7.79 |
| | | $MPV_{20}VBPV_{80}$ | 67.2 | 1.31 | 53.2 | 1.28 | 7.91 |
| | | **$MPV_{30}VBPV_{70}$** | **68.8** | **1.34** | **54.7** | **1.31** | **7.97** |
| | | $MPV_{40}VBPV_{60}$ | 68.3 | 1.33 | 54.4 | 1.31 | 8.01 |
| | | $MPV_{50}VBPV_{50}$ | 67.1 | 1.31 | 53.7 | 1.29 | 7.92 |
| | | $MPV_{60}VBPV_{40}$ | 65.1 | 1.27 | 52.2 | 1.26 | 7.58 |
| | | $MPV_{70}VBPV_{30}$ | 62.7 | 1.22 | 50.5 | 1.21 | 7.30 |
| | | $MPV_{80}VBPV_{20}$ | 59.1 | 1.15 | 47.7 | 1.15 | 6.93 |
| | | $MPV_{90}VBPV_{10}$ | 55.1 | 1.08 | 44.6 | 1.07 | 6.46 |
| | | **$MPV_{100}VBPV_0$** | **51.3** | **1.00** | **41.6** | **1.00** | **6.05** |
| | High | $MPV_0VBPV_{100}$ | 41.4 | 1.40 | 32.6 | 1.36 | 2.41 |
| | | $MPV_{10}VBPV_{90}$ | 41.8 | 1.42 | 32.9 | 1.38 | 2.46 |
| | | **$MPV_{20}VBPV_{80}$** | **42.2** | **1.43** | **33.4** | **1.39** | **2.48** |
| | | $MPV_{30}VBPV_{70}$ | 41.9 | 1.42 | 33.3 | 1.39 | 2.47 |
| | | $MPV_{40}VBPV_{60}$ | 40.4 | 1.37 | 32.2 | 1.35 | 2.35 |
| | | $MPV_{50}VBPV_{50}$ | 38.3 | 1.30 | 30.6 | 1.28 | 2.28 |
| | | $MPV_{60}VBPV_{40}$ | 37.5 | 1.27 | 30.1 | 1.26 | 2.22 |
| | | $MPV_{70}VBPV_{30}$ | 35.5 | 1.20 | 28.6 | 1.19 | 2.14 |
| | | $MPV_{80}VBPV_{20}$ | 32.9 | 1.11 | 26.5 | 1.11 | 1.99 |
| | | $MPV_{90}VBPV_{10}$ | 31.2 | 1.06 | 25.3 | 1.06 | 1.86 |
| | | **$MPV_{100}VBPV_0$** | **29.5** | **1.00** | **23.9** | **1.00** | **1.75** |

electricity load profile, or power grid line properties, as well as a combination of variables to the PV hosting capacity. The workflow can be used to determine the optimal PV portfolios for different local conditions.

A case study using solar irradiance and weather data from Turku, Finland, for two selected days showed that the PV hosting capacity, determined as the maximum fraction of daily PV production and daily electricity consumption, allowed the avoidance of overvoltage events. The largest allowed voltage was set to 1.1 p.u. and the sizes of the PV systems were scaled so that this limit was respected. According to EN 50160 standard [19], the voltage should remain below this limit for 95% of the week and thus this approach leaves marginal for short, especially challenging situations for the power grid. However, it should be noted that other power quality issues beside voltage rise were excluded from this study. The PV hosting capacity of the test power grid was increased by 22–43% when MPV panels (south-facing with a 30° tilt) were replaced with east–west VBPV panels. The production increase was due to a smoother power production profile (i.e., higher daily total production compared to peak production) and high-latitude summer conditions, which highly favored VBPV. It should be noted that the area required for the system also increased, although the area increase was smaller than the production increase. The production was boosted even further, up to 46% compared to MPV with a 30° tilt, by combining MPV and VBPV production.

A more detailed analysis of one of the studied cases (6/2, high-load-size, $MPV_{30}VBPV_{70}$ PV production profile) showed that the maximum allowed PV capacity was limited by short temporal periods (1–30 min), which were characterized by high PV production and sudden variations in the electricity load and/or PV production. This highlights that managing such periods with different voltage regulation devices or allowing over-and undervoltage events to occur in the short term can significantly increase the PV hosting capacity. Active power curtailment and reactive power control by the PV inverters is a potential approach [7].

The key findings of the case study are as follows:

- VBPV and hybrid systems increased the PV hosting capacity of the grid compared to conventional MPV (up to 46%) due to i) higher daily total/daily peak electricity production and ii) the improved temporal match between PV production and electricity consumption.
- The hosting capacity was limited by short (<30 min) moments with high PV production and fluctuating electricity loads. Implementing a suitable curtailment strategy to manage these periods could increase hosting capacity.
- The importance of studying PV as a part of the entire power system, not just as an individual electricity source, is highlighted.

Further work is needed to include more realistic electricity load models and economic analyses in the methodology. Moreover, since the used test network only covered very small geographic area, resulting in low losses in power lines, it was likely to overestimate the absolute values of maximum PV production compared to most real-world distribution grids, although this allowed the comparison of the relative values between different cases. However, further research with different test grids—optimally real distribution grids—is needed to reveal the absolute PV hosting capacities.

## Declaration of Competing Interest

The authors declare that they have no known competing financial interests or personal relationships that could have appeared to influence the work reported in this paper.

## Acknowledgements

The authors acknowledge the financial support from Emil Aaltonen Foundation, Finnish Cultural Foundation, Academy of Finland (research project BioEST, no. 336577) Norwegian Research Council (research project FRIPRO-FRINATEK no. 324243 HELIOS).

## Appendix A. Justification and detailed explanation of the PV curtailment method

A PV power curtailment method described here was applied to the power production profiles. The aim was to eliminate power peaks caused by CEEs close to the peak production time and to keep any other changes to the profiles as small as possible. This curtailment was necessary since the methodology to determine the maximum PV hosting capacity, described in Section 2.2.3, has strong correlation between the peak power production and maximum hosting capacity. Therefore, a CEE that increases the peak power production significantly can lead to underestimation of the hosting

capacity with the production profile, since the total electricity production is increased only marginally. The chosen curtailment method eliminated CEE peaks close to the peak production time and is also easy to implement in practical installations. The detailed procedure is as follows:

1. The modelled power production data of a particular case (day, technology, orientation) referred as $P_{raw}$ is calculated based on DNI and DHI decomposed from measured GHI as described in Section 2.2.2.
2. Clear sky power production data ($P_{CS}$) is calculated for the specific case based on DNI and DHI acquired with Ineichen-Perez clear sky model [22], implemented in PVLIB. All other parameters are the same as in Step 1.
3. The temporal moments when curtailment can be applied are limited to the moments when the corresponding $P_{CS}$ value is at least 85% of the maximum $P_{CS}$ value. The limit was set to 85% since the CEEs occurring below this limit are very unlikely to cause power peaks that increase the daily maximum power production, based on quantitative analysis of the data.
4. For these moments, the curtailment is applied so that the power production cannot exceed the $P_{CS}$ value.

Thus, for any time moment *t*, the curtailed power production *P(t)* can be calculated with Eq. (A1):

$$P(t) = \begin{matrix} P_{raw}(t), if \;\; P_{CS}(t) \leq 0.85 \bullet \max(P_{CS}) \\ \min(P_{raw}(t), P_{CS}(t)), if \;\; P_{CS}(t) \rangle 0.85 \bullet \max(P_{CS}) \end{matrix} \quad \text{(A1)}$$

The effect of the applied filter is illustrated in Fig. A1, which shows raw, clear sky and curtailed profiles for MPV-30 (solid lines) and VBPV (dashed lines). The figure shows that a (likely) CEE that increases the peak production is curtailed off, but no other changes are made. Especially for VBPV, the clear sky production is low around solar noon due to low amount of diffusion in clear sky conditions. This highlights that the curtailment should be done only close to the peak production times.

The effect of the curtailment method is quantitatively shown in Table A1. For the MPV-30 profile, the high peaks around 12 pm are curtailed off, which causes a 5.1% decrease in peak power ($P_{max,A}$) with only marginal 0.2% decrease in energy production ($E_{tot,A}$). As a result, the normalized energy production ($E_{norm}$) increased by 5.1%. For the VBPV profile, $P_{raw} < P_{CS}$ for all datapoints above the curtailment limit, so no curtailment was done.

## Appendix B. The effect of MPV share to the hybrid profile shape.

Table A2
Appendix C Full statistics table for the hybrid systems.
Table A3

## References


[1] Awad, H., Gül, M., 2018. Load-match-driven design of solar PV systems at high latitudes in the Northern hemisphere and its impact on the grid. Sol. Energy 173, 377–397. https://doi.org/10.1016/j.solener.2018.07.010.

[2] Baumann, T., Nussbaumer, H., Klenk, M., Dreisiebner, A., Carigiet, F., Baumgartner, F., 2019. Photovoltaic systems with vertically mounted bifacial PV modules in combination with green roofs. Sol. Energy 190, 139–146. https://doi.org/10.1016/j.solener.2019.08.014.

[3] Baumann, T., Schär, D., Carigiet, F., Dreisiebner, A., Baumgartner, F., 2016. Performance Analysis of PV Green Roof Systems, European Photovoltaic Solar Energy Conference and Exhibition.

[4] Beck, H.E., Zimmermann, N.E., McVicar, T.R., Vergopolan, N., Berg, A., Wood, E. F., 2018. Present and future Köppen-Geiger climate classification maps at 1-km resolution. Sci. Data 5, 1–12. https://doi.org/10.1038/sdata.2018.214.

[5] Böök, H., Poikonen, A., Aarva, A., Mielonen, T., Pitkänen, M.R.A., Lindfors, A.V., 2020. Photovoltaic system modeling: A validation study at high latitudes with implementation of a novel DNI quality control method. Sol. Energy 204, 316–329. https://doi.org/10.1016/j.solener.2020.04.068.

[6] Broderick, R., Quiroz, J., Grijalva, S., Reno, M., Coogan, K., 2014. GridPV Toolbox.

[7] Carigiet, F., Niedrist, M., Scheuermann, C., Baumgartner, F., 2016. Case study of a low-voltage distribution grid with high PV penetration in Germany and simulation analyses of cost-effective measures. Prog. Photovolt. Res. Appl. 24, 1523–1532. https://doi.org/10.1002/PIP.2710.

[8] Chaudhary, P., Rizwan, M., 2018. Voltage regulation mitigation techniques in distribution system with high PV penetration: A review. Renew. Sustain. Energy Rev. 82, 3279–3287. https://doi.org/10.1016/j.rser.2017.10.017.

[9] Dugan, R.C., McDermott, T.E., 2011. An open source platform for collaborating on smart grid research. IEEE Power and Energy Society General Meeting 1–7. https://doi.org/10.1109/PES.2011.6039829.

[10] Fachrizal, R., Ramadhani, U.H., Munkhammar, J., Widén, J., 2021. Combined PV–EV hosting capacity assessment for a residential LV distribution grid with smart EV charging and PV curtailment. Sustainable Energy Grids Networks 26, 100445. https://doi.org/10.1016/j.segan.2021.100445.

[11] Gandhi, O., Kumar, D.S., Rodríguez-Gallegos, C.D., Srinivasan, D., 2020. Review of power system impacts at high PV penetration Part I: Factors limiting PV penetration. Sol. Energy 210, 181–201. https://doi.org/10.1016/j.solener.2020.06.097.

[12] Hartvigsson, E., Odenberger, M., Chen, P., Nyholm, E., 2021. Estimating national and local low-voltage grid capacity for residential solar photovoltaic in Sweden, UK and Germany. Renew. Energy 171, 915–926. https://doi.org/10.1016/J.RENENE.2021.02.073.

[13] Jouttijärvi, S., Lobaccaro, G., Kamppinen, A., Miettunen, K., 2022. Benefits of bifacial solar cells combined with low voltage power grids at high latitudes. Renew. Sustain. Energy Rev. 161, 112354 https://doi.org/10.1016/J.RSER.2022.112354.

[14] Jouttijärvi, S., Tok, M., Karttunen, L., Huerta Medina, H., Ranta, S., Miettunen, K., 2022b. Modeling and Measuring the Power Output of Vertical Bifacial Solar Panels in Nordic Conditions. 8th World Conference on Photovoltaic Energy Conversion 507–511. https://doi.org/10.4229/WCPEC-82022-3BO.14.2.

[15] Kalair, A., Abas, N., Kalair, A.R., Saleem, Z., Khan, N., 2017. Review of harmonic analysis, modeling and mitigation techniques. Renew. Sustain. Energy Rev. 78, 1152–1187. https://doi.org/10.1016/J.RSER.2017.04.121.

[16] Kharrazi, A., Sreeram, V., Mishra, Y., 2020. Assessment techniques of the impact of grid-tied rooftop photovoltaic generation on the power quality of low voltage distribution network - A review. Renew. Sustain. Energy Rev. 120, 109643 https://doi.org/10.1016/J.RSER.2019.109643.

[17] King, D.L., Boyson, W.E., Kratochvil, J.A., 2004. Photovoltaic array performance model, Sandia Report No. 2004-3535. https://doi.org/10.2172/919131.

[18] Lobaccaro, G., Carlucci, S., Croce, S., Paparella, R., Finocchiaro, L., 2017. Boosting solar accessibility and potential of urban districts in the Nordic climate: a case study in Trondheim. Sol. Energy 149, 347–369. https://doi.org/10.1016/j.solener.2017.04.015.

[19] Masetti, C., 2010. Revision of European Standard EN 50160 on power quality: Reasons and solutions. ICHQP 2010 – 14th International Conference on Harmonics and Quality of Power. https://doi.org/10.1109/ICHQP.2010.5625472.

[20] Nguyen, A., Velay, M., Schoene, J., Zheglov, V., Kurtz, B., Murray, K., Torre, B., Kleissl, J., 2016. High PV penetration impacts on five local distribution networks using high resolution solar resource assessment with sky imager and quasi-steady state distribution system simulations. Sol. Energy 132, 221–235. https://doi.org/10.1016/j.solener.2016.03.019.

[21] Nussbaumer, H., Janssen, G., Berrian, D., Wittmer, B., Klenk, M., Baumann, T., Baumgartner, F., Morf, M., Burgers, A., Libal, J., Mermoud, A., 2020. Accuracy of simulated data for bifacial systems with varying tilt angles and share of diffuse radiation. Sol. Energy 197, 6–21. https://doi.org/10.1016/j.solener.2019.12.071.

[22] Perez, R., Ineichen, P., Moore, K., Kmiecik, M., Chain, C., George, R., Vignola, F., 2002. A new operational model for satellite-derived irradiances: description and validation. Sol. Energy 73, 307–317. https://doi.org/10.1016/S0038-092X(02)00122-6.

[23] Ranta, S., Huerta, H., Huhtala, O., Heinonen, A., Stein, J.S., 2020. Modeling Tool Validation for the Yield Prediction of Bifacial East West Vertical System in Nordic Conditions. 37th European Photovoltaic Solar Energy Conference (EUPVSEC) 1460–1465.

[24] Sa'ed, J.A., Wari, Z., Abughazaleh, F., Dawud, J., Favuzza, S., Zizzo, G., 2020. Effect of demand side management on the operation of PV-integrated distribution systems. Appl. Sci. 10 (21), 7551.

[25] Sampath Kumar, D., Gandhi, O., Rodríguez-Gallegos, C.D., Srinivasan, D., 2020. Review of power system impacts at high PV penetration Part II: potential solutions and the way forward. Sol. Energy 210, 202–221. https://doi.org/10.1016/j.solener.2020.08.047.

[26] Schneider, K.P., Mather, B.A., Pal, B.C., Ten, C.W., Shirek, G.J., Zhu, H., Fuller, J. C., Pereira, J.L.R., Ochoa, L.F., de Araujo, L.R., Dugan, R.C., Matthias, S., Paudyal, S., McDermott, T.E., Kersting, W., 2018. Analytic considerations and design basis for the IEEE distribution test feeders. IEEE Trans. Power Syst. 33, 3181–3188. https://doi.org/10.1109/TPWRS.2017.2760011.

[27] Starke, A.R., Lemos, L.F.L., Barni, C.M., Machado, R.D., Cardemil, J.M., Boland, J., Colle, S., 2021. Assessing one-minute diffuse fraction models based on worldwide climate features. Renew. Energy 177, 700–714. https://doi.org/10.1016/J.RENENE.2021.05.108.

[28] Starke, A.R., Lemos, L.F.L., Boland, J., Cardemil, J.M., Colle, S., 2018. Resolution of the cloud enhancement problem for one-minute diffuse radiation prediction. Renew. Energy 125, 472–484. https://doi.org/10.1016/J.RENENE.2018.02.107.

[29] Stein, J.S., Holmgren, W.F., Forbess, J., Hansen, C.W., 2016. PVLIB: open source photovoltaic performance modeling functions for Matlab and Python. In: Conference Record of the IEEE Photovoltaic Specialists Conference. Institute of Electrical and Electronics Engineers Inc., pp. 3425–3430. https://doi.org/10.1109/PVSC.2016.7750303

[30] Sun, X., Khan, M.R., Deline, C., Alam, M.A., 2018. Optimization and performance of bifacial solar modules: A global perspective. Appl. Energy 212, 1601–1610. https://doi.org/10.1016/j.apenergy.2017.12.041.

[31] Utrillas, M.P., Martinez-Lozano, J.A., 1994. Performance evaluation of several versions of the Perez tilted diffuse irradiance model. Sol. Energy 53, 155–162. https://doi.org/10.1016/0038-092X(94)90476-6.

[32] Uzum, B., Onen, A., Hasanien, H.M., Muyeen, S.M., 2020. Rooftop solar PV penetration impacts on distribution network and further growth factors—a comprehensive review. Electronics (Basel) 10, 55. https://doi.org/10.3390/ELECTRONICS10010055.

[33] Viana, M.S., Manassero, G., Udaeta, M.E.M., 2018. Analysis of demand response and photovoltaic distributed generation as resources for power utility planning. Appl. Energy 217, 456–466. https://doi.org/10.1016/j.apenergy.2018.02.153.

[34] Yang, D., 2022. Estimating 1-min beam and diffuse irradiance from the global irradiance: A review and an extensive worldwide comparison of latest separation models at 126 stations. Renew. Sustain. Energy Rev. 159, 112195 https://doi.org/10.1016/J.RSER.2022.112195.

[35] Yang, D., 2016. Solar radiation on inclined surfaces: corrections and benchmarks. Sol. Energy 136, 288–302. https://doi.org/10.1016/J.SOLENER.2016.06.062.